Probability Density Function of Underwater Bomb Trajectory Deviation Due to Stochastic Ocean Surface Slope

Peter C. Chu[1]
e-mail: pcchu@nps.edu

Chenwu Fan

Naval Ocean Analysis and Prediction Laboratory,
Naval Postgraduate School,
Monterey, CA 93943

Ocean wave propagation causes random change in an ocean surface slope and in turn affects the underwater bomb trajectory deviation (r) through a water column. This trajectory deviation is crucial for the clearance of obstacles such as sea mines or a maritime improvised explosive device in coastal oceans using bombs. A nonlinear six degrees of freedom (6DOF) model has been recently developed and verified at the Naval Postgraduate School with various surface impact speeds and surface slopes as model inputs. The surface slope (s) randomly changes between 0 and $\pi/2$ with a probability density function (PDF) p(s), called the s-PDF. After s is discretized into I intervals by $s_1, s_2, \ldots, s_i, \ldots, s_{I+1}$, the 6DOF model is integrated with a given surface impact speed (v_0) and each slope s_i to get bomb trajectory deviation $\hat{r}_i$ at depth (h) as a model output. The calculated series of $\{\hat{r}_i\}$ is re-arranged into monotonically increasing order (r_j} . The bomb trajectory deviation r within (r_j, r_{j+1}) may correspond to one interval or several intervals of s. The probability of r falling into (r_j, r_{j+1}) can be obtained from the probability of s and in turn the PDF of r, called the r-PDF. Change in the r-PDF versus features of the s-PDF, water depth, and surface impact speed is also investigated.
[DOI: 10.1115/1.4003378]

Keywords: 3D underwater bomb trajectory model, probability density function, bomb trajectory deviation, stochastic ocean surface slope, 6DOF model, STRIKE35

1 Introduction

Movement of a fast-moving rigid body such as a bomb through a water column has been studied recently [1–3]. These studies have been motivated by a new concept of using the Joint Direct Attack Munition (JDAM) (i.e., a "smart" bomb guided to its target by an integrated inertial guidance system coupled with a global positioning system) Assault Breaching System (JABS) for mine/maritime improvised explosive device (IED) clearance in order to reduce the risk to personnel and to decrease the sweep timeline without sacrificing effectiveness (Fig. 1). Underwater bomb trajectory depends largely on the surface impact speed and angle. When the surface impact of a high-speed rigid body such as a scaled MK-84 warhead is normal or near normal to the flat water surface, four types of trajectories have been identified from experimental and numerical modeling results [4] depending on the characteristics of the warheads: with tail section and four fins (type 1), with tail section and two fins (type 1I), with tail section and no fin (type 1II), and with no tail section (type IV) (Fig. 2).

The reason for using the four types is the frequent occurrence of the tail/fin separation from the bomb after it enters the water surface. Type-1 trajectories are stably downward without oscillation and tumbling regardless if the water entry velocity is high or low. Type-2 and type-3 trajectories are first downward, then make 180 deg turn (upward), and travel toward the surface. The upward move of type-2 and type-3 warheads is caused by the hydrodynamic instability of the water-body interaction [1,3]. Type-IV trajectories are at first downward with a little horizontal drift and then tumble downward with a large horizontal drift.

The horizontal distance (r) (called trajectory deviation) between the surface impact point and the bomb location varies with depth in different types of trajectories (Fig. 3). This parameter draws attention to naval research due to the threat of mines and maritime IEDs. The prediction of trajectory deviation of an underwater bomb contributes to the bomb breaching for mine and maritime IED clearance in surf and very shallow water zones with depth shallower than 12.2 m (i.e., 40 ft), shallow water zones (12.2–91.4 m, i.e., 40–300 ft), and deep zones (deeper than 91.4 m, i.e., 300 ft) according to U.S. Navy's standards. The bombs' trajectory drift is required to satisfy the condition, $r \leq 2.1$ m, for the validity of mine clearance using bombs [5].

In coastal oceans, waves form when the water surface is disturbed, for example, by wind or gravitational forces. During such disturbances, energy and momentum are transferred to the water mass and the sea-state is changed. For very shallow and shallow water regions, the bottom topography affects the waves dramatically and causes a significant change in surface slope. When a bomb strikes on the wavy ocean surface, a scientific problem arises: How does a randomly changing ocean surface slope affect the underwater bomb trajectory and orientation? Or what is the probability density function of the underwater bomb trajectory deviation due to the random sea surface slope? The major task of this paper is to answer these questions. The effect of the surface slope on the underwater bomb trajectory is presented in Sec. 2. Stochastic features of the sea slope are simply described in Sec. 3. A recently developed six degrees of freedom (6DOF) model at the Naval Postgraduate School for predicting underwater bomb location and trajectory is depicted in Sec. 4. The PDF of bomb's horizontal drift is described in Sec. 5. Sensitivity studies are described in Sec. 6. The conclusions are presented in Sec. 7.

[1]Corresponding author.

Contributed by the Dynamic Systems Division of ASME for publication in the JOURNAL OF DYNAMIC SYSTEMS, MEASUREMENT, AND CONTROL. Manuscript received April 5, 2010; final manuscript received November 23, 2010; published online March 23, 2011. Assoc. Editor: Sheng-Guo Wang.

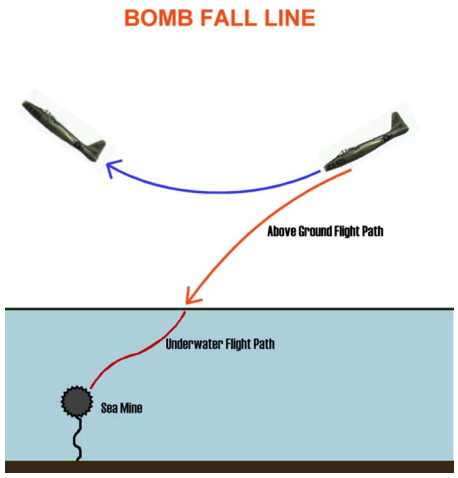

Fig. 1 The concept of airborne sea mine/maritime IED clearance

2 Effect of Ocean Surface Slope on Underwater Bomb Trajectory

Ocean surface slope is usually due to the existence of ocean waves. Let (a, s^*) be the wave amplitude and slope, μ be the inclination angle of the ocean surface,

$$s^* = \tan \mu \tag{1}$$

and ϕ be the bomb impact angle relative to the normal direction of the ocean surface (Fig. 4). For a flat surface (no waves),

$$\mu = 0 \tag{2a}$$

For 90 deg bomb striking (vertically downward),

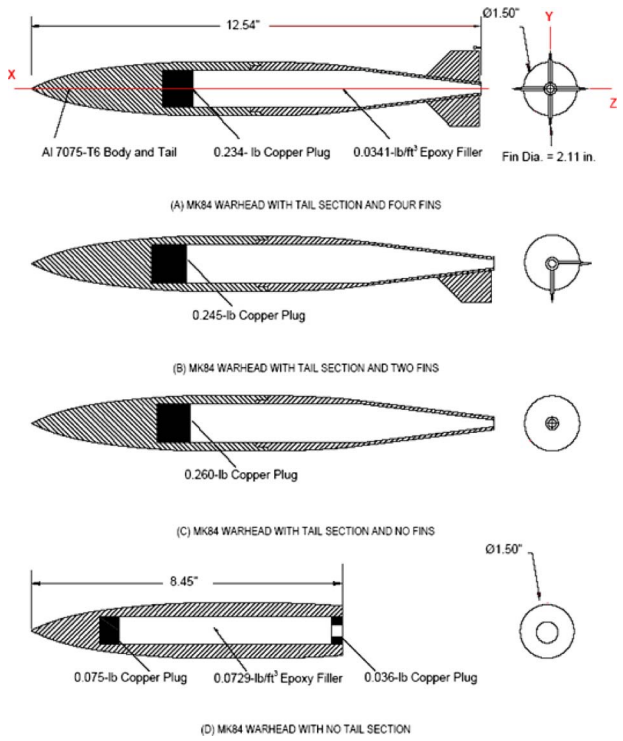

Fig. 2 MK-84 warhead with (*a*) tail section and four fins, (*b*) tail section and two fins, (*c*) tail section and no fins, and (*d*) no tail section

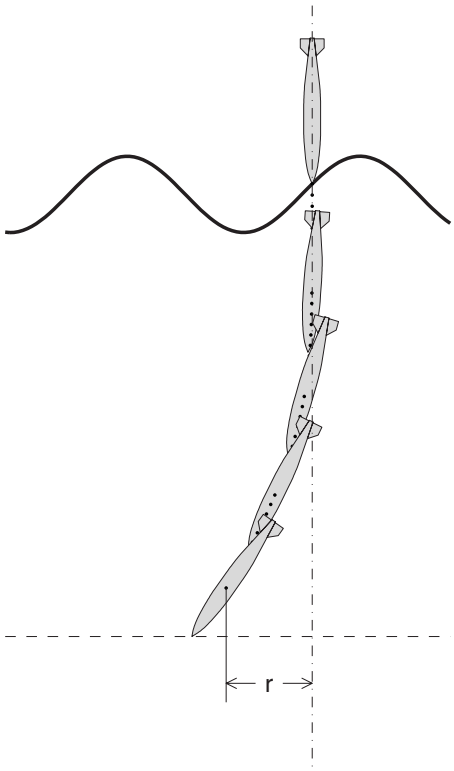

Fig. 3 Dependence of underwater bomb trajectory, orientation, and horizontal deviation (r) on the ocean surface slope or on different locations of the waves

$$\phi = 0 \tag{2b}$$

The ocean waves may cause evident slant of the ocean surface with $\mu \approx 55$ deg [6], which affects the underwater bomb trajectory, orientation, and horizontal drift (r) (Fig. 3). The differential effects depend on which part of the wave is impacted by the bomb (i.e., different sea slopes). Obviously, such a wave effect can be investigated by a 6DOF model with a sloping surface (i.e., μ changing with time) and non-normal impact angle (i.e., $\phi \neq 0$).

Besides, the surface slope also affects the tail separation due to the bomb and cavity orientations and the air-cavity geometry. This is because the air cavitation or supercavitation is usually generated after the bomb enters the water surface [7]. The cavity is usually oriented in the same direction of the bomb velocity, with its geometry simply represented by a cone with the angle (γ). The bomb orientation relative to the cavity is represented by the angle between the bomb main axis and velocity (β). The condition for bomb not hitting the cavity wall is given by (Fig. 5(a)),

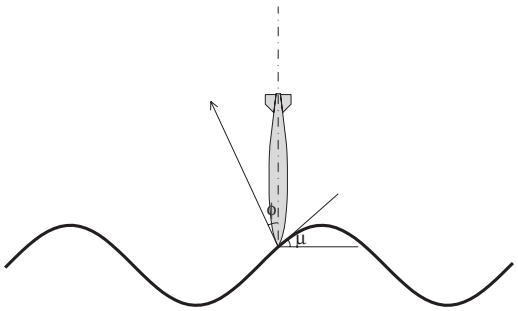

Fig. 4 Ocean surface inclination angle (μ) and bomb impact angle (ϕ) relative to the normal direction of the surface

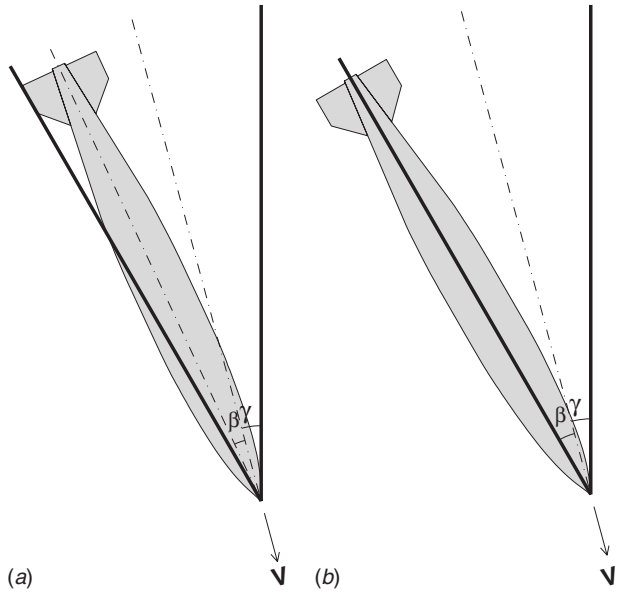

Fig. 5 Air cavity (*a*) with $\beta<\gamma$ (tail section not hitting the cavity wall) and (*b*) with $\beta=\gamma$ (tail section hitting the cavity wall)

$$\beta < \gamma \tag{3a}$$

Violation of condition (3) may cause tail separation (bomb hitting the cavity wall), as shown in Fig. 5(*b*). Ocean waves not only affect the bomb trajectory and orientation but also change the cavity orientation, which may cause

$$\beta > \gamma \tag{3b}$$

i.e., the bomb may hit the cavity wall and cause tail separation (Fig. 6).

3 Ocean Surface Gravity Waves

3.1 Ocean Wave Spectra. Ocean waves are produced by the wind. The faster the wind, the longer the wind blows, and the bigger the area over which the wind blows, the bigger the waves. In determining the sea-state, we wish to know the biggest waves produced by a given wind speed. Suppose the wind blows at certain speed over a large area of the sea. What will be the spectrum of ocean waves at the downwind side of the area? A wave spectrum is the distribution of wave energy as a function of frequency. It describes the total energy transmitted by a wave-field at a given time. Formally, it is given by

$$S(\omega) = 4\int_0^\infty R(\tau)\cos 2\pi\tau d\tau \tag{4}$$

where ω is the frequency of the waves (defined previously) and $R(\tau)$ is the autocorrelation function of the time series of the water-surface elevation (η),

$$R(\tau) = \langle \eta(t)\,\eta(t+\tau)\rangle \tag{5}$$

where τ is the time lag between samples, and bracket means average. Wave spectra are strongly influenced by the wave-producing wind and its statistical/spatial characteristics. The spatial variability is primarily encapsulated into the fetch. Fetch is the length over which the wind blows to generate the waves. Various idealized spectra have been developed. Among them, perhaps the simplest is the Pierson–Moskowitz spectrum [8],

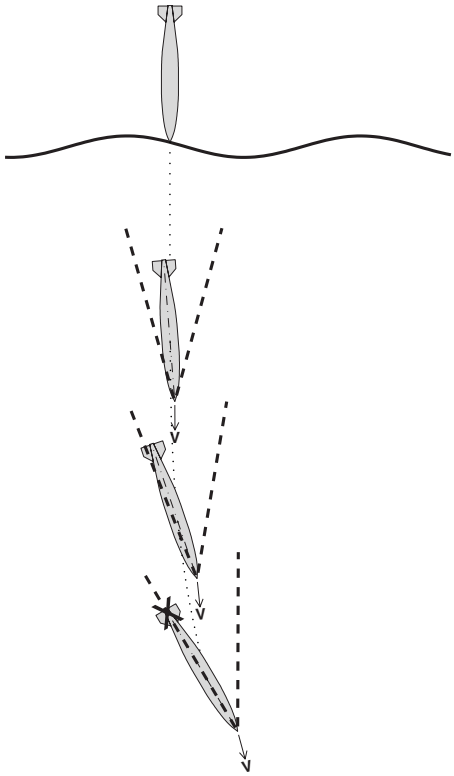

Fig. 6 Wave effect on the air-cavity orientation, which may cause $\beta>\gamma$ (tail section hitting the cavity wall)

$$S(\omega) = \frac{\alpha_1 g^2}{\omega^5}\exp\left[-\alpha_2\left(\frac{\omega_0}{\omega}\right)^4\right] \tag{6}$$

which was established using the assumption that if the wind blew steadily for a long time over a large area, the waves would come into equilibrium with the wind. Here, g is the gravitational acceleration, $\alpha_1=8.1\times10^{-3}$, $\alpha_2=0.74$, $\omega_0=g/U_{19.5}$, and $U_{19.5}$ is the wind speed at a height of 19.5 m above the sea surface, the height of the anemometers on the weather ships. The Pierson–Moskowitz spectrum is based on the concept of a fully developed sea (a sea produced by winds blowing steadily over hundreds of miles for several days). Here, a long time is roughly 10,000 wave periods, and a "large area" is roughly 5000 wavelengths on a side.

Wave spectrum is never fully developed. After analyzing data collected during the Joint North Sea Wave Observation Project (JONSWAP), a wave spectrum was proposed for the wave development stage through nonlinear wave-wave interactions even for very long times and distances [9],

$$S(\omega) = \frac{\alpha_3 g^2}{\omega^5}\exp\left[-\frac{5}{4}\left(\frac{\omega_p}{\omega}\right)^4\right]\alpha_4^r,\quad r=\exp\left[-\frac{(\omega-\omega_p)^2}{2\alpha_5^2\omega_p^2}\right] \tag{7}$$

which is called the JONSWAP spectrum. Here, the constants were determined using the wave data collected during the JONSWAP experiment,

$$\alpha_3 = 0.076\left(\frac{U_{10}^2}{Ag}\right)^{0.22},\quad \omega_p = 22\left(\frac{g^2}{U_{10}A}\right)^{1/3},\quad \alpha_4 = 3.3$$

$$\alpha_5 = \begin{cases} 0.07 & \omega \le \omega_p \\ 0.09 & \omega > \omega_p \end{cases} \tag{8}$$

where A is the fetch and U_{10} is the wind speed at a height of 10 m above the sea surface. The mean square slope s^{*2} is calculated from a wave spectrum. For the JONSWAP spectrum, it is around 0.024 [9].

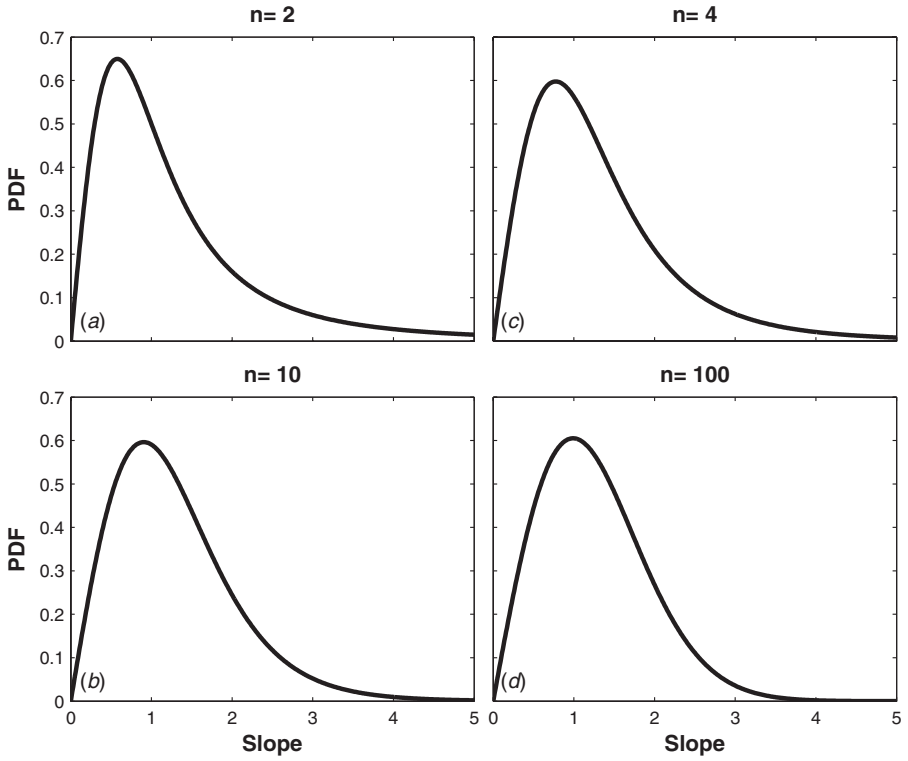

Fig. 7 The s-PDFs for various surface characteristics: (*a*) *n*=2, (*b*) *n*=4, (*c*) *n*=10, and (*d*) *n*=100

3.2 PDF of Ocean Surface Slope. Ocean waves can also be treated as a stochastic process that can be expressed in terms of one or more random variables, such as the wave amplitude, wave period, wavelength, and surface slope. For example, the PDF of the wave amplitude a (defined as half the crest-to-trough wave height) is given by the well-known Rayleigh distribution [10],

$$p(a) = \frac{a}{m_0}\exp\left(-\frac{a^2}{m_0^2}\right) \tag{9}$$

where m_0 is the root-mean square of surface amplitude, i.e., the root of the 0th moment of the energy spectrum. For very strong winds, the Weibull distribution for a wave amplitude fits data better than the Rayleigh distribution [11].

Similarly, the PDF of the wave period T_m satisfies the Rayleigh distribution for a narrow spectrum [10] and the Weibull distribution for a wide spectrum [12]. Combining the two types, a more general form (Weibull distribution) of PDF for the wave period T_m was proposed [13],

$$p(T_m) = \frac{(2n-1)^{n/2}}{\Gamma(n/2)2^{n-2}}T_m^{2n-1}\exp\left[-\frac{(2n-1)}{4}T_m^4\right] \tag{10}$$

where n is a parameter related to the spectral width and Γ is the gamma function. When n=2, Eq. (10) corresponds to the Rayleigh distribution. Using the dispersion relation for surface gravity waves in deep water, the PDF for the wavelength λ was obtained [13],

$$p(\lambda) = \frac{2(n-1)^{n/2}}{\Gamma(n/2)2^{n/2}\lambda_m^n}\lambda^{n-1}\exp\left[-\frac{(n-1)}{2\lambda_m^2}\lambda^2\right] \tag{11}$$

where λ_m is the most probable wavelength.

With the independent assumption between wave amplitude and wavelength, the PDF of the averaged wave slope s^* scaled by its standard deviation σ (the real slope is $s^*=s\sigma$) was derived from the PDF of wavelength and the PDF of wave amplitude [13],

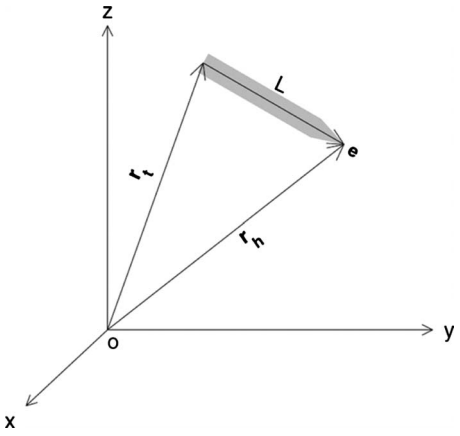

Fig. 8 Position vectors r_h and r_t and the unit vector e (from Chu et al. 2010 [4])

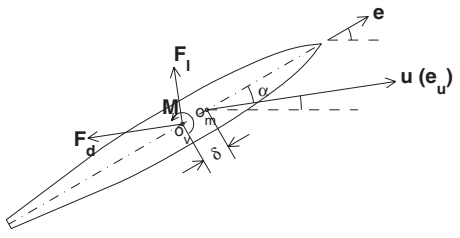

Fig. 9 Attack angle (α), center of volume (o_v), center of mass (o_m), and drag and lift forces (exerted on o_v). Note that δ is distance between o_v and o_m with positive (negative) value when the direction from o_v to o_m is the same (opposite) as the unit vector e. The unit vector e_u is in the direction of the bomb velocity (from Chu et al. 2010 [4]).

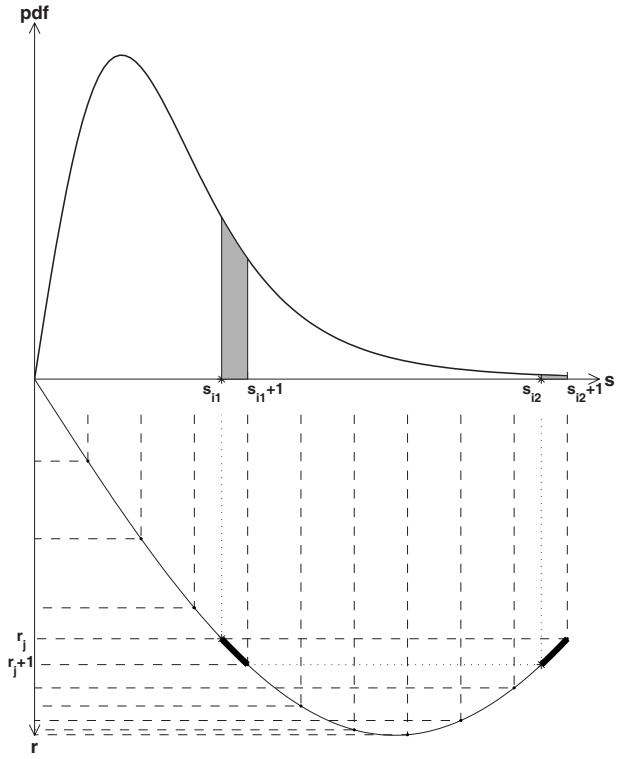

Fig. 10 Calculation of the probability for the bomb's horizontal drift *r* taking values between r_j and r_{j+1} from *m* intervals of surface slope s. Here, *m*=1 and *m*=2.

$$p(s) = \frac{n}{(n-1)} s \left[1 + \frac{s^2}{(n-1)} \right]^{-(n+2)/2} \tag{12}$$

Generally speaking, the peakedness of slopes (s^*) is generated by nonlinear wave-wave interactions in the range of gravity waves, and the skewness of slopes is generated by nonlinear coupling between the short waves and the underlying long waves. For $n=2$, the PDF of the wave period corresponds to the Rayleigh distribution (see Eq. (9)). For $n=10$, the PDF in Eq. (12) fits the Gram–Charlier distribution [14] very well in the range of small slopes. As $n \to \infty$, the PDF of wavelength (11) tends to the Gaussian distribution [13]. Figure 7 shows four typical surface-slope characteristics: (a) $n=2$, (b) $n=4$, (c) $n=10$, and $n=100$. It is seen that there is almost no difference in PDF between $n=10$ and $n=100$.

4 A 6DOF Model (STRIKE35)

Recently, a 6DOF model has been developed at the Naval Postgraduate School for predicting underwater object location and trajectory. It contains four parts: three basic unit vectors, momentum equation, moment of momentum equation, and semi-empirical formulas for drag, lift, and torque coefficients [15–21].

4.1 Three Unit Vectors. Let the earth-fixed coordinate system be used with the unit vectors $(\mathbf{i}, \mathbf{j})$ in the horizontal plane and the unit vector $\mathbf{k}$ in the vertical direction. The two end-points of the bomb (i.e., head and tail points) are represented by $\mathbf{r}_h(t)$ and $\mathbf{r}_t(t)$. The difference between the two vectors in the nondimensional form

$$\mathbf{e} = \frac{\mathbf{r}_h - \mathbf{r}_t}{|\mathbf{r}_h - \mathbf{r}_t|} \tag{13}$$

is the unit vector representing the body's main axis direction (Fig. 8). The centers of mass (o_m) and volume (o_v) are located on the main axis with δ the distance between o_v and o_m, which has a positive (negative) value when the direction from o_v to o_m is the same (opposite) as the unit vector $\mathbf{e}$. Let α be the angle of attack between the direction of the main body axis ($\mathbf{e}$) and the direction of the body velocity ($\mathbf{e}_u$) [21] (Fig. 9). The location (called translation) of the bomb is represented by the position of o_m,

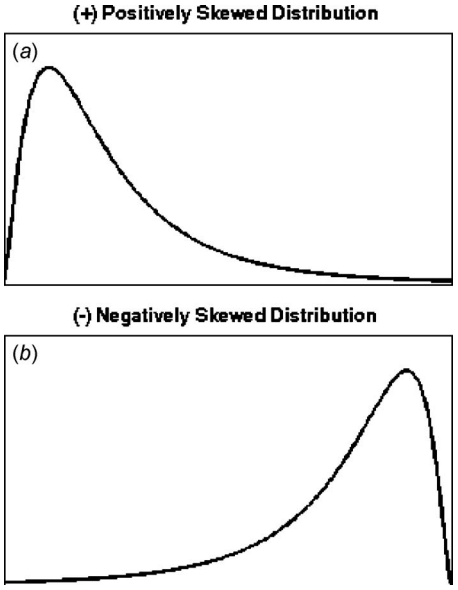

Fig. 11 (*a*) Positively and (*b*) negatively skewed PDFs

$$\mathbf{r}(t) = x\mathbf{i} + y\mathbf{j} + z\mathbf{k} \tag{14}$$

The translation velocity is given by

$$\frac{d\mathbf{r}_o}{dt} = \mathbf{u}, \quad \mathbf{u} = U\mathbf{e}_u \tag{15}$$

where $(U, \ \mathbf{e}_u)$ are the speed and unit vector of the bomb velocity. Let $\mathbf{V}_w$ be the water velocity. Water-to-body relative velocity $\mathbf{V}$ (called the relative velocity) is represented by

$$\mathbf{V} \equiv \mathbf{V}_w - \mathbf{u} \approx -\mathbf{u} = -U\mathbf{e}_u \tag{16}$$

Here, the water velocity is assumed much smaller than the rigid-body velocity. A third basic unit vector ($\mathbf{e}_m^h$) can be defined perpendicular to both $\mathbf{e}$ and $\mathbf{e}_u$,

$$\mathbf{e}_m^h = \frac{\mathbf{e}_u \times \mathbf{e}}{|\mathbf{e}_u \times \mathbf{e}|} \tag{17}$$

4.2 Momentum Equation. The momentum equation of a bomb is given by

$$m\frac{d\mathbf{u}}{dt} = \mathbf{F}_g + \mathbf{F}_b + \mathbf{F}_d + \mathbf{F}_l \tag{18}$$

where m is the mass of the rigid body, $\mathbf{u}$ is the translation velocity of the center of mass,

$$\mathbf{F}_g = -mg\mathbf{k}, \quad \mathbf{F}_b = \rho \Pi g \mathbf{k} \tag{19}$$

are the gravity and buoyancy force, Π is the volume of the rigid body, $\mathbf{k}$ is the unit vector in the vertical direction (positive upward), and g is the gravitational acceleration. $\mathbf{F}_d$ is the drag force

$$\mathbf{F}_d = -f_d \mathbf{e}_u \tag{20}$$

and $\mathbf{F}_l$ is the lift force

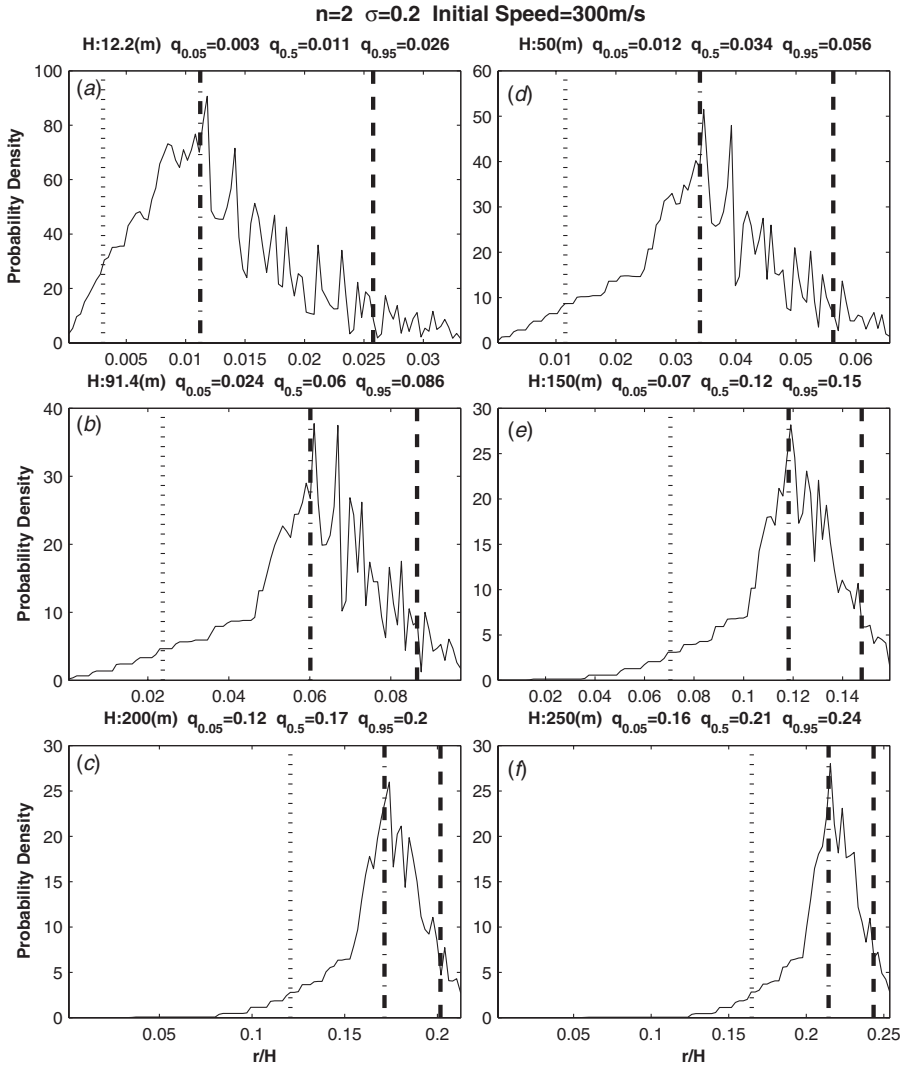

Fig. 12 Probability distribution of the bomb's horizontal drift (scaled by the depth) r/H with $n=2$, $\sigma=0.2$, and $V=300$ m/s for various depths: (*a*) 12.2 m (i.e., 40 ft), (*b*) 50 m, (*c*) 91.4 m (i.e., 300 ft), (*d*) 150 m, (*e*) 200 m, and (*f*) 250 m

$$\mathbf{F}_l = f_l \mathbf{e}_l, \quad \mathbf{e}_l = \mathbf{e}_m^h \times \mathbf{e}_u, \quad \mathbf{e}_m^h = \frac{\mathbf{e}_u \times \mathbf{e}}{|\mathbf{e}_u \times \mathbf{e}|} \tag{21}$$

where f_d and f_l are the magnitudes of the forces and $\mathbf{e}_u$ is the unit vector of the bomb velocity. The magnitudes (f_d, f_l) are represented by the drag law,

$$f_d = \tfrac{1}{2} C_d \rho A_w U^2, \quad f_l = \tfrac{1}{2} C_l \rho A_w U^2 \tag{22}$$

where ρ is the water density, A_w is the underwater projection area, and (C_d, C_l) are the drag and lift coefficients, which are determined by the experiments.

4.3 Moment of Momentum Equation. The moment of momentum equation of a bomb is given by

$$\mathbf{J} \cdot \frac{d\mathbf{\Omega}}{dt} = -\delta \mathbf{e} \times (\rho \Pi g \mathbf{k}) + \mathbf{M}_h \tag{23}$$

where $\mathbf{\Omega}$ is the rigid body's angular velocity vector, $\mathbf{M}_\mathrm{h}$ is the hydrodynamic torque due to the drag/lift forces, and $\mathbf{J}$ is the gyration tensor. Since the drag/lift forces are exerted on the center of volume (o_v), the hydrodynamic torque (relative to the center of mass, o_m) $\mathbf{M}_h$ is computed by

$$\mathbf{M}_h = -\delta \mathbf{e} \times (\mathbf{F}_d + \mathbf{F}_l) - n \delta_f \mathbf{e} \times \mathbf{F}_c^f + \mathbf{M}_\mathrm{tr} + \mathbf{M}_\mathrm{rot} \tag{24}$$

where the first two terms in the right hand side represent the torque by the drag and lift forces, $\mathbf{F}_c^f$ is the combined drag and lift forces on a pair of fins, n is the number of pairs of fins, and δ_f is the distance between o_v and the center of mass of the pair of fins, which has a positive (negative) value when the direction from o_v to that center is the same (opposite) as the unit vector $\mathbf{e}$. $\mathbf{M}_\mathrm{tr}$ is the antitranslation torque by the moment of drag/lift forces, and $\mathbf{M}_\mathrm{rot}$ is the antirotation torque. $\mathbf{M}_\mathrm{tr}$ is perpendicular to both $\mathbf{e}_u$ (the direction of $\mathbf{u}$) and $\mathbf{e}$ (the body orientation), and therefore it is in the same direction of the unit vector $\mathbf{e}_m^h$,

$$\mathbf{M}_\mathrm{tr} = M_\mathrm{tr} \mathbf{e}_m^h \tag{25}$$

with M_tr being its magnitude calculated by the drag law,

$$M_\mathrm{tr} = \tfrac{1}{2} C_m \rho A_w L_w U^2 \tag{26}$$

Here, C_m is the antitranslation torque coefficient.

The antirotation torque ($\mathbf{M}_\mathrm{rot}$) is decomposed into two parts,

Table 1 The median horizontal drift (unit: m) of an underwater bomb at various depths obtained from ensemble integration of the 6DOF model with various input parameters

Depth (m)	Case 1: V=300 m/s, n=2, σ=0.2	Case 2: V=300 m/s, n=2, σ=0.02	Case 3: V=300 m/s, n=100, σ=0.2	Case 4: V=300 m/s, n=100, σ=0.02	Case 5: V=300 m/s, n=2, σ=1.0	Case 6: V=200 m/s, n=2, σ=0.2
12.2	0.16	0.02	0.16	0.02	0.37	0.17
50.0	1.7	0.41	1.8	0.31	3.1	2.5
91.4	5.4	1.01	5.7	1.19	8.6	8.9
150.0	18.0	7.2	18.0	7.95	22.5	25.5
200.0	34.0	19.2	34.0	20.0	42.0	44.0
250.0	52.5	35.0	55.0	37.5	62.5	65.0

$$\mathbf{M}_{\text{rot}} = \mathbf{M}_s + \mathbf{M}_c \tag{27}$$

where the torque $\mathbf{M}_s$ (resistant to self-spinning, $\Omega_s\mathbf{e}$) parallels the main axis of the body (i.e., the unit vector $\mathbf{e}$),

$$\mathbf{M}_s = -M_s\mathbf{e} \tag{28}$$

and the torque $\mathbf{M}_c$ is perpendicular to the unit vector $\mathbf{e}$,

$$\mathbf{M}_c = -M_c\mathbf{e}_\omega, \quad \mathbf{e}_\omega \perp \mathbf{e} \tag{29}$$

where M_s and M_c are the corresponding scalar parts. The drag law shows that [15]

$$M_s = \tfrac{1}{2}C_s\rho A_w L_w^3|\Omega_s|\Omega_s \tag{30}$$

$$M_c = \tfrac{1}{2}CF(\mu)\rho A_w L_w V_r^2, \quad \mu \equiv \Omega L_w/V_r \tag{31}$$

where the function $F(\mu)$ is obtained from the surface integration of torque due to cross-body hydrodynamic force (perpendicular to the body) [22],

$$F(\mu) \equiv \begin{cases} \dfrac{1}{6\mu} & \text{for } \mu \geq 1/2 \\ \left[\left(\dfrac{1}{4}-\mu^2\right)+\dfrac{4}{3}\mu^2+\dfrac{1}{2\mu^2}\left(\dfrac{1}{16}-\mu^4\right)\right] & \text{for } \mu < 1/2 \end{cases} \tag{32}$$

Here, V_r is the projection of the water-to-body relative velocity on the vector $\mathbf{e}_r=\mathbf{e}_\omega\times\mathbf{e}$. Using Eq. (16), we have

$$V_r = \mathbf{V}\cdot\mathbf{e}_r = -U\mathbf{e}_u\cdot(\mathbf{e}_\omega\times\mathbf{e}) \tag{33}$$

4.4 Drag/Lift/Torque Coefficients. The drag/lift/torque coefficients should be given before running the 6DOF model. These coefficients depend on various physical processes such as water-surface penetration, super-cavitation, and bubble dynamics. A diagnostic-photographic method has been developed [4] to get semi-empirical formulas for calculating the drag/lift/torque coefficients for underwater bombs with dependence on the angle of attack (α), rotation rate along the bomb's major axis (Ω), and Reynolds number, $\text{Re}=UD/\nu$ (with D as the effective diameter of the bomb and ν as the water viscosity) [21],

$$C_d = 0.02 + 0.35e^{-2(\alpha-\pi/2)^2}\left(\frac{\text{Re}}{\text{Re}^*}\right)^{0.2} + 0.008\Omega\sin\theta \tag{34}$$

$$C_l = \begin{cases} 0.35\sin(\theta_1)\left(\dfrac{\text{Re}}{\text{Re}^*}\right)^{0.2} & \text{if } \alpha \leq \dfrac{\pi}{2} \\ 0.1\sin(\theta_2) - 0.015\Omega\left(\dfrac{\text{Re}}{\text{Re}^*}\right)^2\sin(\theta_2^{0.85}) & \text{if } \alpha > \dfrac{\pi}{2} \end{cases} \tag{35}$$

$$C_m = \begin{cases} 0.07\sin(2\alpha)\left(\dfrac{\text{Re}^*}{\text{Re}}\right)^{0.2} & \text{if } \alpha \leq \dfrac{\pi}{2} \\ 0.02\sin(2\alpha)\sqrt{\left(\dfrac{\text{Re}}{\text{Re}^*}\right)} & \text{if } \alpha > \dfrac{\pi}{2} \end{cases} \tag{36}$$

Here, $\text{Re}^*=1.8\times10^7$ is the critical Reynolds number, and

Table 2 The values of $q_{0.95}$ for the horizontal drift (unit: m) of an underwater bomb at various depths obtained from ensemble integration of the 6DOF model with various input parameters

Depth (m)	Case 1: V=300 m/s, n=2, σ=0.2	Case 2: V=300 m/s, n=2, σ=0.02	Case 3: V=300 m/s, n=100, σ=0.2	Case 4: V=300 m/s, n=100, σ=0.02	Case 5: V=300 m/s, n=2, σ=1.0	Case 6: V=200 m/s, n=2, σ=0.2
12.2	0.32	0.06	0.27	0.04	0.54	0.17
50.0	2.8	0.85	2.55	0.65	4.0	3.6
91.4	7.86	3.02	7.40	2.47	10.05	10.97
150.0	22.5	9.60	21.0	11.1	25.5	28.5
200.0	40.0	26.0	38.0	26.0	46.0	48.0
250.0	60.0	45.0	60.0	42.5	67.5	70.0

Table 3 The values of $q_{0.05}$ for the horizontal drift (unit: m) of an underwater bomb at various depths obtained from ensemble integration of the 6DOF model with various input parameters

Depth (m)	Case 1: V=300 m/s, n=2, σ=0.2	Case 2: V=300 m/s, n=2, σ=0.02	Case 3: V=300 m/s, n=100, σ=0.2	Case 4: V=300 m/s, n=100, σ=0.02	Case 5: V=300 m/s, n=2, σ=1.0	Case 6: V=200 m/s, n=2, σ=0.2
12.2	0.13	0.003	0.05	0.005	0.15	0.04
50.0	0.6	0.06	0.80	0.08	1.8	1.05
91.4	5.48	0.125	7.40	0.35	5.76	5.30
150.0	10.5	3.9	12.45	4.50	18.0	18.0
200.0	24.0	13.6	26.0	14.8	34.0	32.0
250.0	40.0	27.5	45.0	30.0	55.0	55.0

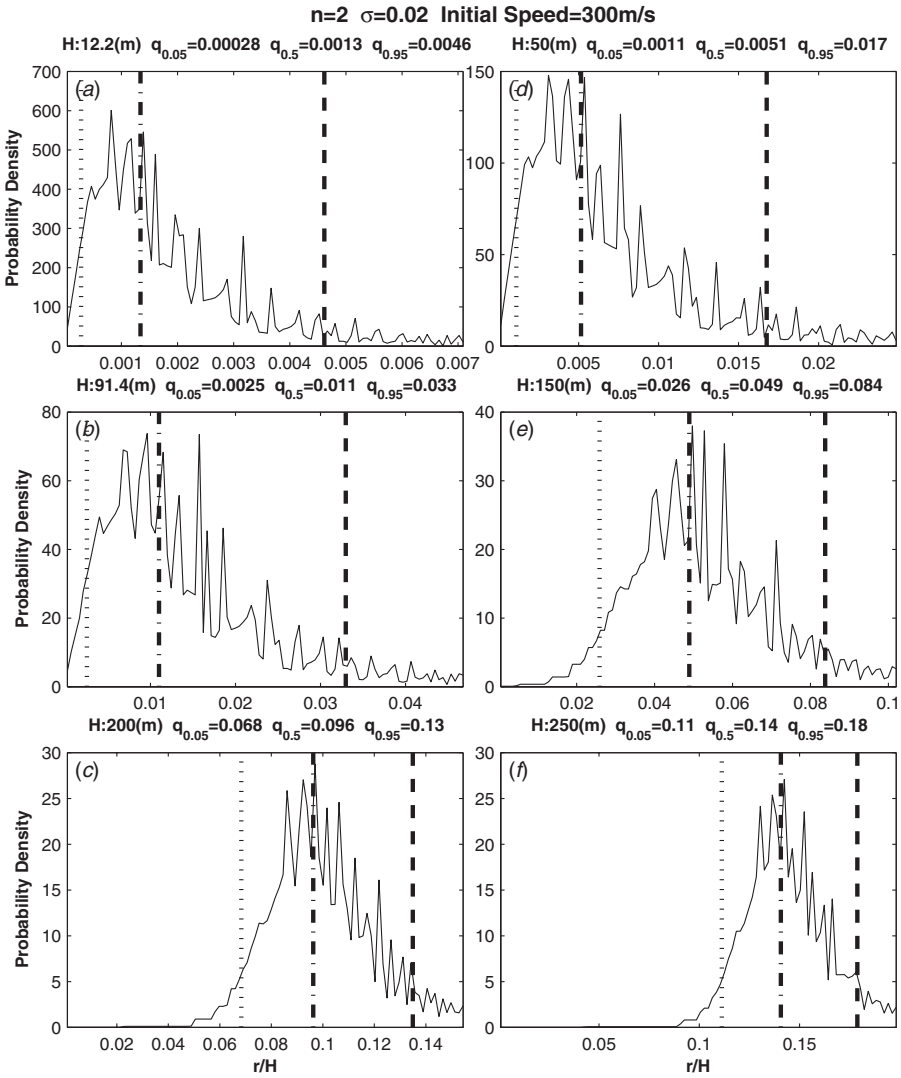

Fig. 13 Probability distribution of the bomb's horizontal drift (scaled by the depth) r/H with $n=2$, $\sigma=0.02$, and $V=300$ m/s for various depths: (*a*) 12.2 m (i.e., 40 ft), (*b*) 50 m, (*c*) 91.4 m (i.e., 300 ft), (*d*) 150 m, (*e*) 200 m, and (*f*) 250 m

$$\theta \equiv (\pi^{2.2} - (\pi - |\pi - 2\alpha|)^{2.2})^{1/2.2} \operatorname{sgn}(\pi - 2\alpha) \tag{37}$$

$$\theta_1 = \pi\left(\frac{2\alpha}{\pi}\right)^{1.8}, \quad \theta_2 = 2\pi\left(\frac{2\alpha}{\pi} - 1\right)^{0.7} \tag{38}$$

The drag/lift and torque coefficients are valid for other sizes, but the same shape is described in Fig. 2.

The 6DOF model is highly nonlinear and solved numerically. The angle of attack (α), rotation rate along the bomb's major axis (Ω), and Reynolds number (Re) depend heavily on the bomb's velocity and orientation, and therefore they are recalculated at each time step.

5 PDF of Bomb's Horizontal Drift

Let the bomb be dropped in the vertical direction to the slanted sea surface characterized by an averaged slope ($s^*=\sigma s$) in a wave period; here, $s^*=\tan\mu$ (see Fig. 3). Obviously, the horizontal drift depends on the types of the warheads. Since a JDAM usually has a tail section with four fins, we concentrate only on the type-1 warheads in this study. Consider a five-time s^* value as the interval $[0,5s^*]$ for the change in the surface slope. This interval $[0,5s^*]$ is divided into I equal subintervals,

$$\sigma s_i = \frac{5is^*}{I}, \quad i = 0,1,2,\ldots,I \tag{39}$$

with the corresponding inclination,

$$\mu_i = \arctan(\sigma s_i) = \arctan\frac{5is^*}{I}, \quad i = 0,1,2,\ldots,I \tag{40}$$

For a given parameter n in the s-PDF, the probability for s^* taking values between σs_{i-1} and σs_i is calculated by

$$P_i \equiv \text{Prob}(s_i \le s \le s_{i+1}) = \int_{s_i}^{s_{i+1}} p(s)ds \tag{41}$$

The 6DOF model is integrated I times (called ensemble integration) from the surface impact speed (V) and various μ_i values to get the bomb horizontal drift $\hat{r}_i$ ($i=0,1,\ldots,I$) at depth $z=-H$. The series $\{\hat{r}_i, i=0,1,\ldots,I\}$ might not be in monotonically increasing or decreasing order. Therefore, it is reorganized into monotonically increasing order $\{r_j, j=0,1,\ldots,J\}$, with $J \le I$. The inequality is due to an interval $[r_j, r_{j+1}]$ of the horizontal drift corresponding to m intervals $\{[s_{i1}, s_{i1}+1],[s_{i2}, s_{i2}$

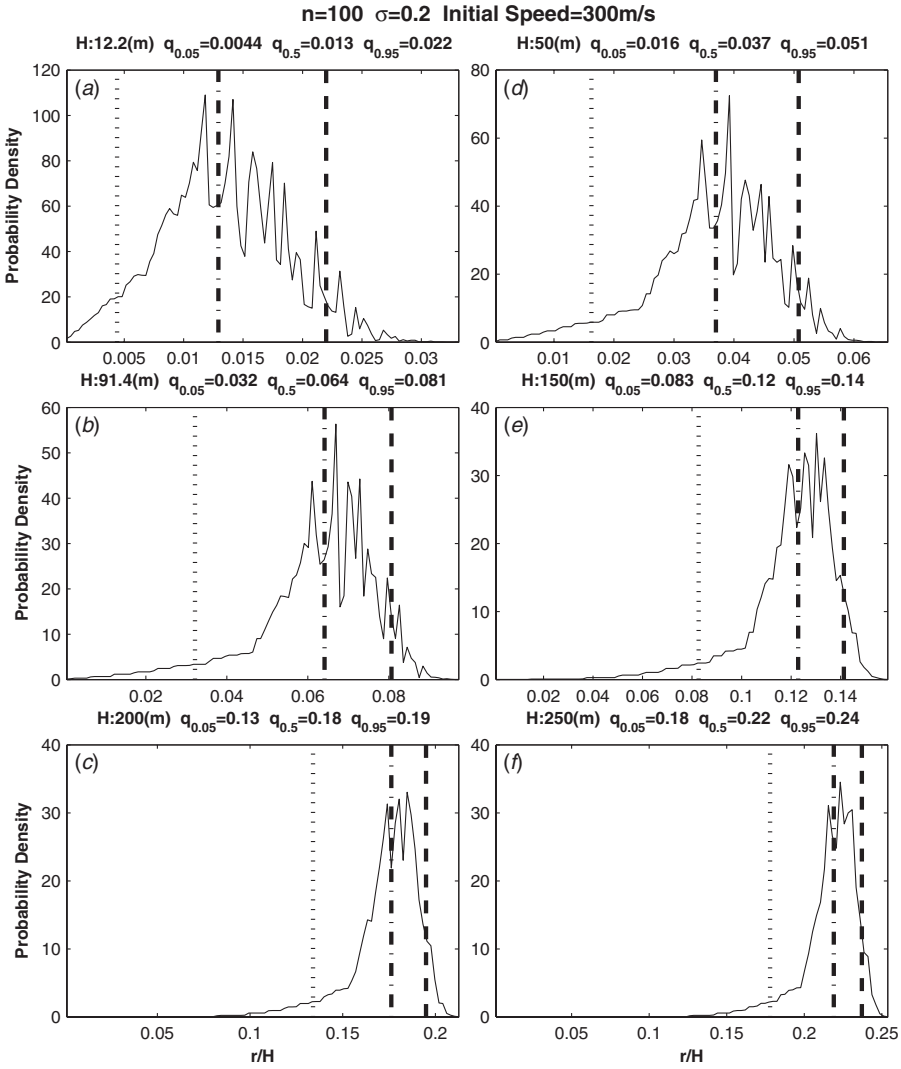

Fig. 14 Probability distribution of the bomb's horizontal drift (scaled by the depth) r/H with $n=100$, $\sigma=0.2$, and $V=300$ m/s for various depths: (*a*) 12.2 m (i.e., 40 ft), (*b*) 50 m, (*c*) 91.4 m (i.e., 300 ft), (*d*) 150 m, (*e*) 200 m, and (*f*) 250 m

$+1],\ldots,[s_{im},s_{im}+1]\}$ of the surface slope (Fig. 10). The probability for the bomb's horizontal drift r taking values between r_j and r_{j+1} is calculated by

$$Q_j \equiv \text{Prob}(r_j \le r \le r_{j+1}) = \int_{s_{i1}}^{s_{i1+1}} p(s)ds + \int_{s_{i2}}^{s_{i2+1}} p(s)ds + \cdots + \int_{s_{in}}^{s_{in+1}} p(s)ds \tag{42}$$

The probability density between r_j and r_{j+1} is calculated by

$$p_j = \frac{Q_j}{r_{j+1} - r_j} \tag{43}$$

From p_j, we can obtain the PDF of r, called the r-PDF.

From a given r-PDF, several useful parameters can be easily determined such as the median (50 percentile $q_{0.5}$), 95 percentile ($q_{0.95}$), and skewness. The skewness is defined with respect to the third moment about the mean. The positive (negative) skewness indicates the long tail of the r-PDF pointing to the large (small) r-values. Since the Gaussian distribution is nonskewed, identification of the skewness provides useful information about the most probable horizontal drift r. For negative skewness, long tail points to the larger r-values, and the most probable horizontal drift r is in the smaller area. On the other hand, for positive skewness, the long tail points to the smaller r-values, and the most probable horizontal drift r is in the larger area (Fig. 11).

6 Sensitivity Studies

6.1 Dependence of the *r*-PDF on Depth. Dependence of r-PDF on depth can be identified from the ensemble integration ($I=100$) of the 6DOF model with given bomb's surface impact speed ($V=300$ m/s), $s^*=0.2$ (i.e., $\sigma=0.2$), and $n=2$ (i.e., large peakedness in the s-PDF). The calculated r-PDF (Fig. 12) is positively skewed for shallow depth ($H=12.2$ m, i.e., 40 ft), reduces the skewness as depth increases to 50 m, and becomes negatively skewed as the depth exceeds 91.4 m (i.e., 300 ft). The negative skewness strengthens as the depth becomes deeper than 91.4 m. The horizontal axis in all the panels in Fig. 12 is the nondimensional horizontal drift r/H. The median (50 percentile $q_{0.5}$) of the horizontal drift (r) is 0.16 m at the depth $z=-12.2$ m, 1.7 m at $z=-50$ m, 5.4 m at $z=-91.4$ m (300 ft), 18.0 m at $z=-150$ m, 34.0 m at $z=-200$ m, and 52.5 m at $z=-250$ m (Table 1). Here, z is the vertical coordinates with $z=0$ corresponding to the water surface. Thus, down to the depth of 50 m, the median value of the

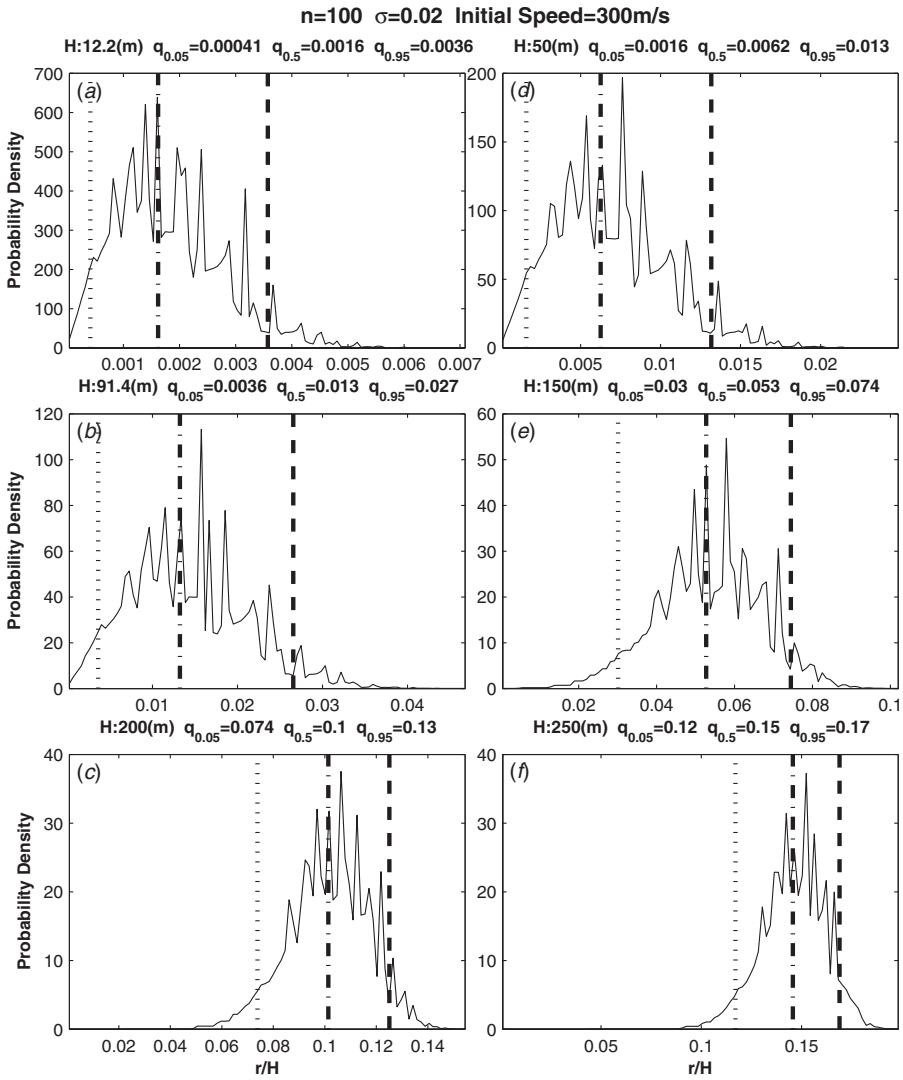

Fig. 15 Probability distribution of the bomb's horizontal drift (scaled by the depth) r/H with $n=100$, $\sigma=0.02$, and $V=300$ m/s for various depths: (*a*) 12.2 m (i.e., 40 ft), (*b*) 50 m, (*c*) 91.4 m (i.e., 300 ft), (*d*) 150 m, (*e*) 200 m, and (*f*) 250 m

horizontal drift is always less than the Navy's criterion, i.e., 2.1 m. The 95 percentile ($q_{0.95}$) of the horizontal drift (r) represents a reasonable estimation (with 95% of confidence) of the distance between bomb and mine/maritime IED when the bomb maneuvers in the water column. If this value is smaller than 2.1 m, according to the Navy's standard, the bomb will effectively "kill" the mine/maritime IED. It is 0.32 m at the depth $z=-12.2$ m, 2.8 m at $z=-50$ m, 7.86 m at $z=-91.4$ m (300 ft), 22.5 m at $z=-150$ m, 40.0 m at $z=-200$ m, and 60.0 m at $z=-250$ m (Table 2). The 5 percentile ($q_{0.05}$) of the horizontal drift (r) represents the minimum distance (likely) between bomb and mine/maritime IED when the bomb maneuvers in the water column. It is 0.13 m at the depth $z=-12.2$ m, 0.6 m at $z=-50$ m, 5.48 m at $z=-91.4$ m (300 ft), 10.5 m at $z=-150$ m, 24.0 m at $z=-200$ m, and 40.0 m at $z=-250$ m (Table 3).

For a small standard deviation of the surface slope ($\sigma=0.02$) with keeping the same values for other parameters as Fig. 12 (i.e., $V=300$ m/s, $n=2$), the calculated r-PDF (Fig. 13) is positively skewed for depth from $H=12.2$ m (i.e., 40 ft) to H=91.4 m (i.e., 300 ft), reducing the skewness as depth increases to 250 m. The median (50 percentile $q_{0.5}$) of the horizontal drift (r) is 0.02 m at the depth $z=-12.2$ m, 0.41 m at $z=-50$ m, 1.01 m at $z=-91.4$ m (300 ft), 7.2 m at $z=-150$ m, 19.2 m at $z=-200$ m, and 35.0 m at $z=-250$ m (Table 1). Thus, down to the depth of 91.4 m (300 ft), the median value of the horizontal drift is always less than the Navy's criterion, i.e., 2.1 m. The 95 percentile ($q_{0.95}$) of the horizontal drift (r) is 0.06 m at the depth $z=-12.2$ m, 0.85 m at $z=-50$ m, 3.02 m at $z=-91.4$ m (300 ft), 9.6 m at $z=-150$ m, 26.0 m at $z=-200$ m, and45.0 m at $z=-250$ m (Table 2).

6.2 Dependence of the *r*-PDF on the Peakedness of the *s*-PDF. Keeping all the initial conditions in running the 6DOF model the same as described in Fig. 12 (i.e., $V=300$ m/s, $\sigma=0.2$) except changing the parameter n of the s-PDF from 2 to 100 (small peakedness), the ensemble integration of the 6DOF model shows the following results. The calculated r-PDF (Fig. 14) is almost zero skewness for shallow depths ($H=12.2$ m, 50 m) and becomes negatively skewed as the depth becomes 91.4 m (i.e., 300 ft). The negative skewness strengthens as the depth becomes deeper than 91.4 m. Comparing Figs. 14 and 12, we may find that the negative skewness of r-PDF increases as n increases. The median, $q_{0.95}$, and $q_{0.05}$ of the horizontal drift (r) do not change too much as n increases from 2 to 100 (Tables 1–3).

For small standard deviation of the surface slope ($\sigma=0.02$) with keeping the same values for other parameters as Fig. 14 (i.e., V

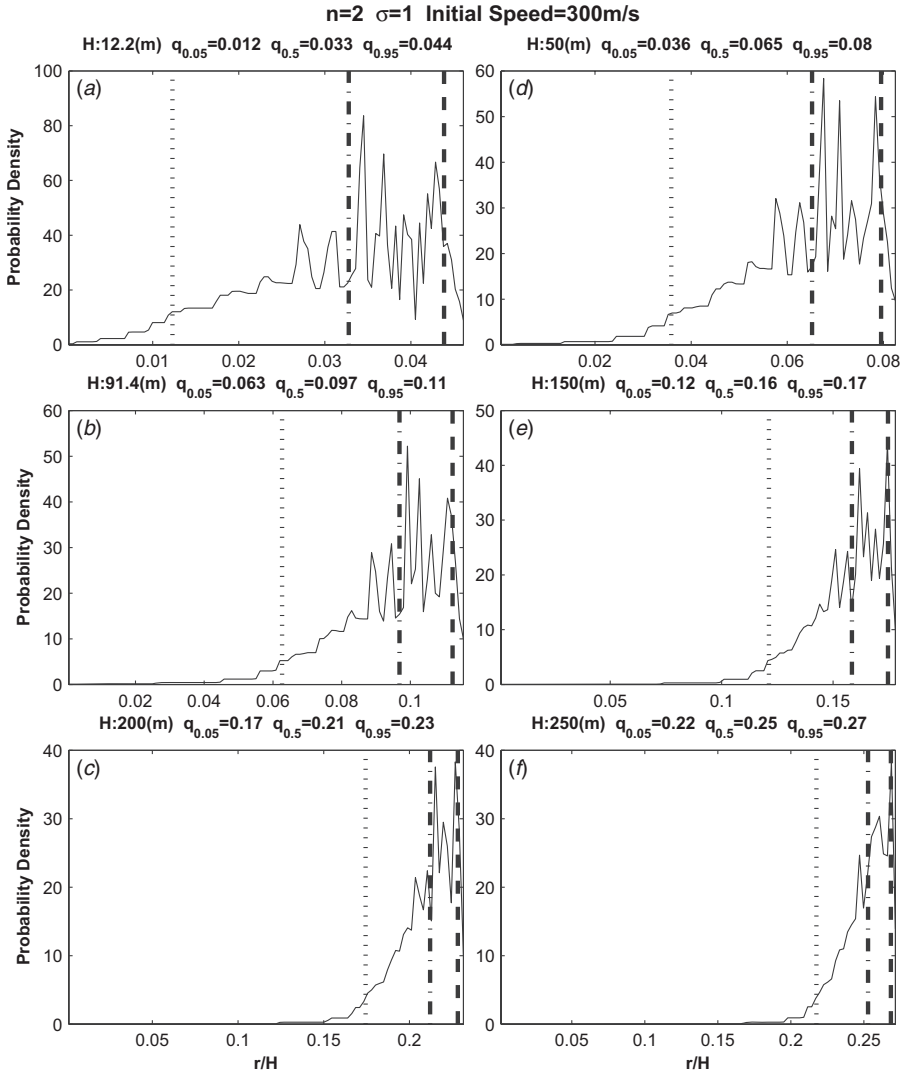

Fig. 16 Probability distribution of the bomb's horizontal drift (scaled by the depth) r/H with $n=2$, $\sigma=1.0$, and $V=300$ m/s for various depths: (*a*) 12.2 m (i.e., 40 ft), (*b*) 50 m, (*c*) 91.4 m (i.e., 300 ft), (*d*) 150 m, (*e*) 200 m, and (*f*) 250 m

$=300$ m/s, $n=100$), the calculated r-PDF (Fig. 15) is positively skewed for depth from $H=12.2$ m (i.e., 40 ft) to H=91.4 m (i.e., 300 ft), reducing the skewness as the depth increases to 250 m. Comparing Figs. 15 and 14, we may find that the positive skewness of r-PDF increases as σ decreases. The median, $q_{0.95}$, and $q_{0.05}$ of the horizontal drift (r) reduces as σ decreases from 0.2 to 0.02 (Tables 1–3).

6.3 Dependence of the r-PDF on the Standard Deviation of Surface Slope σ. Keeping all the initial conditions in running the 6DOF model the same as described in Sec. 6.1 except increasing the averaged surface slope σ from 0.2 to 1, the calculated r-PDF (Fig. 16) is negatively skewed at all depths, and the negative skewness enhances as the depth increases. Comparing Figs. 16 and 12, we may find that the negative skewness of r-PDF increases as σ increases. The median, $q_{0.95}$, and $q_{0.05}$ of the horizontal drift (r) increase drastically as σ increases from 0.2 to 1.0 (Tables 1–3). For example, $q_{0.95}$ is 0.54 m at depth z=−12.2 m, 4.0 m at z=−50 m, 10.05 m at z=−91.4 m (300 ft), 25.5 m at z=−150 m, 46.0 m at z=−200 m, and 67.5 m at z=−250 m (Table 2).

6.4 Dependence of the r-PDF on the Surface Impact Speed V. Keeping all the initial conditions in running the 6DOF model the same as those described in Sec. 6.1 except decreasing the surface impact speed from 300 m/s to 200 m/s, the calculated r-PDF (Fig. 17) is quite comparable to the case with the impact speed of 300 m/s (Fig. 12) such as positive skewness for shallow depth ($H=12.2$ m, i.e., 40 ft), weaker skewness as depth increasing to 50 m, and negative skewness as the depth exceeding 91.4 m (i.e., 300 ft). Comparing Figs. 17 and 12, reduction in surface impact speed leads to the increase in the peakedness of the r-PDF. The median, $q_{0.95}$, and $q_{0.05}$ of the horizontal drift (r) are usually higher for $V=200$ m/s than that for $V=300$ m/s except for the very shallow water depth (z=−12.2 m) where $q_{0.95}$ and $q_{0.05}$ are lower for $V=200$ m/s (0.17 m, 0.04 m) than that for $V=300$ m/s (0.32 m, 0.13 m) (Tables 1–3).

7 Conclusions

The PDF of the horizontal drift of underwater bomb trajectory (i.e., r-PDF) due to stochastic ocean surface slope is obtained through ensemble integration of the 6DOF model recently developed at the Naval Postgraduate School. For a bomb dropping in

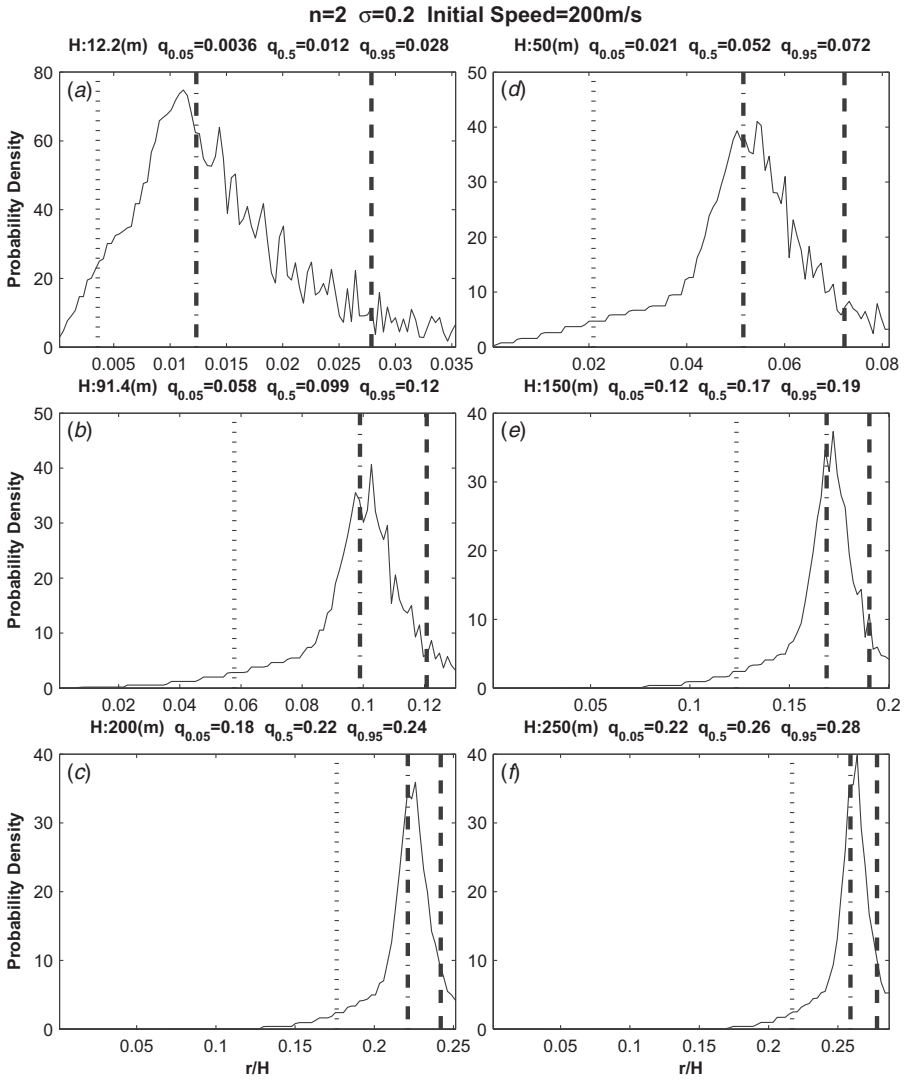

Fig. 17 Probability distribution of the bomb's horizontal drift (scaled by the depth) r/H with $n=2$, $\sigma=0.2$, and $V=200$ m/s for various depths: (*a*) 12.2 m (i.e., 40 ft), (*b*) 50 m, (*c*) 91.4 m (i.e., 300 ft), (*d*) 150 m, (*e*) 200 m, and (*f*) 250 m

the vertical direction to a slanted sea surface, the input parameters of the 6DOF model are the bomb's surface impact speed (V) and surface slope. The surface slope is a random variable depending on two parameters: (a) averaged slope within a wave period (σ) and (b) peakedness of the s-PDF (n). The s-PDF is discretized into I intervals (in this paper, $I=100$). For given values of (V,σ,n), the 6DOF model is integrated I times with different values of the surface slope from the s-PDF to obtained I values of the horizontal drift at various depth. The r-PDF is then constructed from these r-values. The r-PDF has the following features.

(1) The r-PDF varies with depth. Usually, the r-PDF is positively skewed for very shallow water ($H=12.2$ m, i.e., 40 ft) and negatively skewed down below. An increase in the peakedness parameter of the s-PDF (n) or the averaged surface slope in a wave period (σ) reduces the positive skewness at the very shallow water and enhances the negative skewness. A decrease in the bomb's surface impact speed (V) enhances the peakedness of the r-PDF. Three measures were calculated ($q_{0.05}$, $q_{0.5}$, and $q_{0.95}$) from the r-PDF.

(2) The values of $q_{0.95}$ are small for all cases at a very shallow depth (z=−12.2 m, i.e., 40 ft) with a maximum value of 0.54 m for the initial conditions of ($V=300$ m/s, $n=2$, $\sigma=1.0$). This value (0.54 m) is much smaller than the critical value of 2.1 m for effectively "killing" the mine/maritime. This may prove that the JABS is effective to clear mines and light obstacles in very shallow water (depth up to 12.2 m, i.e., 40 ft).

(3) The values of $q_{0.95}$ are all larger than 2.1 m when the depth is deeper than 50 m. This indicates that to extend the JABS from very shallow water (12.2 m depth) to shallow water (12.2–91.4 m) needs more studies.

(4) Usually, a bomb is vertically downward when it hits the ocean surface due to the fast speed in the air column, i.e., $\phi=0$ in this study. For $\phi\neq 0$, it just adds to an extra surface slope as if the bomb would hit the surface vertically. Furthermore, in this study, the water velocity $\mathbf{V}_w$ is neglected versus the bomb velocity $\mathbf{u}$ (see Eq. (16)). This indicates that the influence of underwater flow is not considered. The only influence on the underwater bomb is the ocean surface. This may be true for shallow water depth (less than 91.4 m deep, i.e., 300 ft) since the water velocity is usually less than 1 m/s. We will investigate the influence of the underwater flows in future studies.

Acknowledgment

The Office of Naval Research Breaching Technology Program (Grant No. N0001410WX20165, Program Manager: Brian Almquist) supported this study.

References

[1] Chu, P. C., and Ray, G. P., 2006, "Prediction of High-Speed Rigid Body Maneuvering in Air-Water-Sediment," *Advances in Fluid Mechanics*, M. Rahman and C. A. Brebbia, eds., WIT Press, Southampton, UK, Vol. 6, pp. 43–52.
[2] Ray, G. P., 2006, "Bomb Strike Experiments for Mine Clearance Operations," MS thesis, Meteorology and Physical Oceanography, Naval Postgraduate School, Monterey, CA, p. 197.
[3] Chu, P. C., Fan, C. W., and Gefken, P. R., 2008, "Semi-Empirical Formulas of Drag/Lift Coefficients for High-Speed Rigid Body Maneuvering in Water Column," Adv. Fluid Mech., **7**, pp. 163–172.
[4] Chu, P. C., Bushnell, J. M., Fan, C. W., and Watson, K. P., 2011, "Modeling of Underwater Bomb Trajectory for Mine Clearance," J. Defense Model. Simulation, **8**(1), pp. 25–36.
[5] Humes, G., 2007, Technology Transition Agreement, EC SHD-FYO6-03 FNC Product: Standoff Assault Breaching Weapon Fuze Improvement, Office of Naval Research, Arlington, Virginia, USA, pp. 1–10.
[6] Kinsman, B., 1965, *Wind Waves*, Prentice-Hall, Englewood Cliffs, NJ, p. 676.
[7] Dare, A., Landsberg, A., Kee, A., and Wardlaw, A., 2003, "Three-Dimensional Modeling and Simulation of Weapons Effects for Obstacle Clearance," DoD User Group Conference, Bellevue, WA, Jun. 9–13, p. 9.
[8] Pierson, W. J., Jr., and Moskowitz, L., 1964, "A Proposed Spectral Form for Fully Developed Wind Seas Based on the Similarity Theory of S. A. Kitaigorodskii," J. Geophys. Res., **69**, pp. 5181–5190.
[9] Hasselmann, K., Barnett, T. P., Bouws, E., Carlson, H., Cartwright, D. E., Enke, K., Ewing, J. A., Gienapp, H., Hasselmann, D. E., Kruseman, P., Meerburg, A., Muller, P., Olbers, D. J., Richter, K., Sell, W., and Walden, H., 1973, "Measurements of Wind-Wave Growth and Swell Decay During the Joint North Sea Wave Project (JONSWAP)," Deutsches Hydrographisches Institut, Hamburg, Reihe A, **8**(12), pp. 1–95.
[10] Longuet-Higgins, M. S., 1975, "On the Joint Distribution of the Periods and Amplitudes of Sea Waves," J. Geophys. Res., **80**, pp. 2688–2694.
[11] Forristall, G. Z., 1978, "On the Statistical Distribution of Wave Heights in a Storm," J. Geophys. Res., **83**, pp. 2353–2358.
[12] Bretschneider, C. L., 1959, "Wave Variability and Wave Spectra for Wind-Generated Gravity Waves," U.S. Army Corps of Engineer Beach Erosion Board Technical Memorandum No. 113, pp. 1–192, available from Maury Oceanographic Library, Stennis Space Center, MS.
[13] Liu, Y., Yan, X.-H., Liu, W. T., and Hwang, P. A., 1997, "The Probability Density Function of Ocean Surface Slopes and Its Effects on Radar Backscatter," J. Phys. Oceanogr., **27**, pp. 782–797.
[14] Cox, C. S., and Munk, W. H., 1954, "Measurement of the Roughness of the Sea Surface From Photographs of the Sun's Glitter," J. Opt. Soc. Am., **44**, pp. 838–850.
[15] Chu, P. C., Fan, C. W., Evans, A. D., and Gilles, A., 2004, "Triple Coordinate Transforms for Prediction of Falling Cylinder Through the Water Column," ASME J. Appl. Mech., **71**, pp. 292–298.
[16] Chu, P. C., Gilles, A., and Fan, C. W., 2005, "Experiment of Falling Cylinder Through the Water Column," Exp. Therm. Fluid Sci., **29**, pp. 555–568.
[17] Chu, P. C., and Fan, C. W., 2005, "Pseudo-Cylinder Parameterization for Mine Impact Burial Prediction," ASME J. Fluids Eng., **127**, pp. 1215–1220.
[18] Chu, P. C., and Fan, C. W., 2006, "Prediction of Falling Cylinder Through Air-Water-Sediment Columns," ASME J. Appl. Mech., **73**, pp. 300–314.
[19] Chu, P. C., and Fan, C. W., 2007, "Mine Impact Burial Model (IMPACT35) Verification and Improvement Using Sediment Bearing Factor Method," IEEE J. Ocean. Eng., **32**(1), pp. 34–48.
[20] Chu, P. C., 2009, "Mine Impact Burial Prediction From One to Three Dimensions," Appl. Mech. Rev., **62**(1), p. 010802.
[21] Chu, P. C., Fan, C. W., and Gefken, P. R., 2010, "Diagnostic-Photographic Determination of Drag/Lift/Torque Coefficients of High Speed Rigid Body in Water Column," ASME J. Appl. Mech., **77**, p. 011015.
[22] Rouse, H., 1938, *Fluid Mechanics for Hydraulic Engineers*, McGraw-Hill, New York.